Soil Dynamics and Earthquake Engineering 71 (2015) 128–142

Contents lists available at ScienceDirect

Soil Dynamics and Earthquake Engineering

journal homepage: www.elsevier.com/locate/soildyn

A GLE-based model for seismic displacement analysis of slopes including strength degradation and geometry rearrangement

Valeria Bandini [a], Giovanni Biondi [a,*], Ernesto Cascone [a], Sebastiano Rampello [b]

[a] University of Messina, Messina, Italy
[b] University of Rome La Sapienza, Roma, Italy

ARTICLE INFO

Article history:
Received 3 August 2014
Received in revised form
16 January 2015
Accepted 18 January 2015

Keywords:
Slope displacement analysis
Earthquake-induced displacements
Mass transfer
Cyclic degradation
Shaking table tests

ABSTRACT

Seismic performance of natural slopes, earth structures and solid-waste landfills can be evaluated through displacement-based methods in which permanent displacements induced by earthquake loading are assumed to progressively develop along the critical sliding surface as a result of transient activation of plastic mechanisms within the soil mass. For sliding mechanisms of general shape the earthquake-induced displacements should be computed using a model that provides a closer approximation of sliding surface. When large permanent displacement are induced by seismic actions, due to substantial shear strength reduction, and significant changes in ground surface occur, an improved estimate of permanent displacement can be obtained using a model which accounts for shear strength reduction and mass transfer between adjacent portions of the slope resulting from geometry changes of ground surface during the seismic event.

In this paper, a GLE-based model is proposed for seismic displacement analysis of slopes that accounts for shear strength degradation and for geometry rearrangement. Model accuracy is validated against experimental results obtained from shaking table tests carried out on small scale model slopes. Comparison of computed and experimental results demonstrates the capability of the proposed approach in capturing the main features of the observed seismic response of the model slopes.

1. Introduction

During strong earthquakes soils develop significant deformations that may affect the stability conditions of natural slopes and earth structures possibly causing failures and involving significant losses in terms of damages to environment, structures and lifelines.

Seismic performance of these geotechnical systems can be evaluated through different methods of analysis, ranging from simplified procedures to rigorous numerical methods, thus requiring different levels of accuracy for appropriate problem formulation, modelling of mechanical soil behaviour and analysis procedures.

Among the available approaches to evaluate the seismic stability of slopes, the displacement-based approach represents a good compromise between computational effort and results accuracy and has the advantage of providing a quantitative assessment of earthquake-induced displacement using a rather simple numerical procedure.

Permanent slope displacements induced by earthquake loading can be evaluated using the sliding block analysis, first proposed by Newmark [1], which requires a three-step procedure. First, the critical acceleration, which brings the system to a limit equilibrium condition, and the associated failure mechanism are determined through the pseudo-static approach; then, the equation of motion of the system is derived; finally, for a given acceleration time history, the cumulative displacement of the potential sliding mass is computed by double integration of the equation of motion.

It is worth noting that the displacement analysis is not capable of reproducing the whole deformation pattern of a slope or earth structure but only the displacements due to shear deformations. Volumetric deformation possibly leading to compression and bulging rather than sliding cannot be captured by a Newmark-type computation ([2]). Therefore, the computed permanent displacement should merely be considered as an index of the seismic performance of the slope and not as the actual expected displacement.

In the original formulation of Newmark's sliding block analysis, the effects of possible reduction of soil shear strength and in turn of critical acceleration induced by seismic actions, as well as the effect of changes in slope geometry during the earthquake, are not taken into account.

In the attempt of improving Newmark's approach, studies were carried out dealing with single-, two- or multi-block models or with modified conventional slice methods.

* Correspondence to: Dipartimento di Ingegneria Civile, Informatica, Edile, Ambientale e Matematica Applicata, Contrada di Dio, S. Agata, Messina 98166, Italy. Tel.: +39 90 397 7169; fax: +39 90 397 7480.
E-mail address: gbiondi@unime.it (G. Biondi).

http://dx.doi.org/10.1016/j.soildyn.2015.01.010
0267-7261/

List of symbols

a, $a(t)$ seismic acceleration, time history of seismic acceleration
a_c, $a_c(t)$ critical seismic acceleration, time history of critical seismic acceleration
A_k, B_k, A_{ko}, B_{ko} numerical parameters defined by Eqs. (17)–(20)
c'_i effective cohesion at the base of the ith slice
c_a apparent cohesion at the contact between the geomembranes
C_u, $C_u(t)$ undrained shear strength, time dependent values of undrained shear strength
$C_{u,0}$ initial (static) value of undrained shear strength
$C_{u,i}$, $C_{u,i}(t)$ undrained shear strength available at the base of the ith slice
$C_{u,p}$, $C^*_{u,p}$, $C_{u,r}$ peak, corrected peak and remoulded undrained shear strength
$C_u(N_{i,j})$ undrained shear strength after $N_{i,j}$ significant straining cycles
d, d_y permanent displacement of the block parallel to the base, vertical component of d
D strong motion duration
$\ddot{d}_j$, d_j relative acceleration and displacement of the jth block
$\ddot{d}_r$, d_r relative acceleration and displacement of the reference block
d_0, $d_0(t)$ permanent displacement of a single block sliding on a horizontal plane
d_r displacement of the reference block (parallel to the rth block base)
e_i distance described in Fig. 1
E_i, X_i normal and shear inter-slice forces acting (between the ith and the $(i-1)$th slices)
$f(x_i)$ inter-slice force function
F_f, F_m force (f) and moment (m) pseudo-static safety factor of the slope
F_{PS} pseudo-static safety factor of the slope
g gravity acceleration
G soil shear modulus
$G_{0,i}$ small strain shear modulus at the base of the ith slice at level
$G(\gamma_{c,i})$ values of the G at the base of the ith slice for a given value of the induced shear strain level
h_i distance described in Fig. 1
I_a Arias intensity
k, $k(t)$ seismic acceleration coefficient, time history of seismic acceleration coefficient
k_h, k_v horizontal and vertical component of seismic acceleration coefficient
k_c, $k_c(t)$ critical acceleration coefficient, time history of critical acceleration coefficient
$k_{c(f)}$, $k_{c(m)}$ values of k_c obtained through force or moment limit equilibrium conditions
$k^*_{c,p}$, $k_{c,r}$ values of k_c computed for corrected peak (p) and remoulded (r) values of C_u
l_i length of the base of ith slice (Fig. 1)
n, N number of vertical slices, number of blocks
N'_i normal effective forces acting at the base of the ith slice of the slope
N_c, N_{eq} number of loading cycles, cumulative value of N_c
$N_{i,j}$ number of significant straining cycles
P_d destructiveness potential factor
PI plasticity index
$q_{j,r}$ displacement conversion factor
r_i distance described in Fig. 1
S_r, $S_r(t)$ shape factor, time dependent value of the shape factor
$\overline{T}_j$, $\overline{T}_{j,\,lim}$ driving and resisting shear forces acting at the base of the jth block
U_i, $U_i(t)$ resultant of the pore water pressure at the base of the ith slice
v_i distance described in Fig. 1
w soil water content
$\overline{W}_j$ weight of the jth block
$\overline{W}_r$ weight of the reference block
$\overline{W}_0$ weight of the fictitious block No. 0
W_i, $W_i(t)$ weight of the ith slice, current value of W_i
x_i abscissa of the center of ith slice of the slope
$\overline{\alpha}_j$, $\overline{\alpha}_{j-1}$ inclination of the base of jth and $j-1$th block
δ degradation parameter
ϕ^* interface friction angle at the contact between the geomembranes
φ'_i angle of shearing resistance at the base of the ith slice
$\gamma_c(t)$ cyclic shear strain
$\gamma_{c,i}$, $\gamma_{c,i}(t)$ earthquake-induced shear strain at the base of the ith slice
$\gamma_{m,i}$ mean earthquake-induced shear strain at the base of the ith slice
γ_v volumetric threshold shear strain
$\Delta\tau_{c,i}$, $\Delta\tau_{c,i}(t)$ earthquake-induced shear-stress at the base of the ith slice
Δu earthquake-induced pore pressure
Δu^* earthquake-induced pore pressure ratio
$\Delta u^*_{i,j}$ earthquake-induced pore pressure ratio at the base of the ith slice after the jth significant straining cycle ($N_{i,j}$)
$\Delta u^*_{i,max}$ maximum excess pore pressure ratio at the base of the ith slice
$\varepsilon_{i,j}$ weighting factor for excess pore pressure evaluation
λ percentage of $f(x_i)$ used in the solution
λ_c values of λ obtained searching for minimum critical acceleration coefficient
λ_{PS} values of λ obtained searching for minimum pseudo-static safety factor
σ'_{n0} static effective stress acting normally to the potential sliding surface

Single block models (i.e. the infinite slope scheme), accounting for possible changes of soil shear strength, were derived with reference to both cohesive (e.g.: [3,4]) and saturated cohesionless soils (e.g.: [5–8]).

Two-block (e.g.: [9–11]) or multi-block (e.g.: [12–14]) models, including the effect of changes in slope geometry, were proposed embodying aspects of two-block models proposed for seismic analysis of gravity retaining walls (e.g.: [15,16]). In these models two or more blocks slide along two or more straight-line segments representing the slip surface, and the concept of mass transfer between adjacent blocks is introduced to account for internal deformations satisfying the principle of mass conservation. In most of these models, displacements development requires internal shearing with full mobilisation of shear strength along the inter-block boundaries. Moreover, since the inclinations of inter-block boundaries affect the analysis results, a critical set of boundary inclinations is evaluated minimising the slope critical acceleration. Also, kinematic compatibility of displacements of two adjacent blocks is introduced assuming the velocity vector to be continuous at the contact between them.

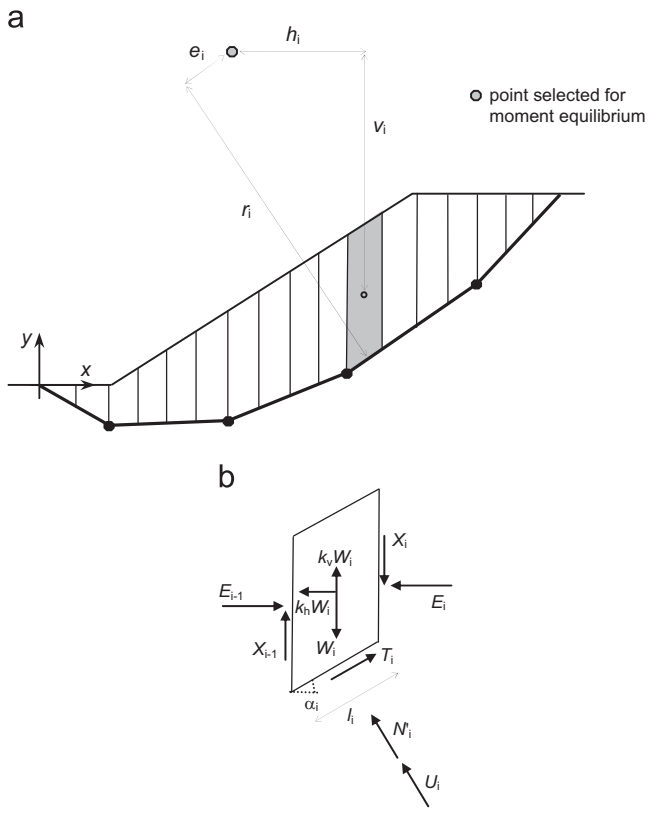

Fig. 1. Slope scheme and notations.

Multi-block models were also derived including both shear strength reduction and geometry rearrangement. In these studies the multi-block approach is coupled with appropriate constitutive models (e.g. [17–19]) or simplified pore water pressure generation models (e.g. [20,21]), or undrained shear strength degradation models (e.g. [22]) consisting in empirical relationships based on large sets of experimental data.

In the last decades, models based on Sarma [e.g. [12], Bishop [e.g. [23–25], Carter [e.g. 23,24], Janbu [e.g. [26] and Fredlund and Krahn [e.g. [27,21] slice methods of stability analysis were finally developed in the attempt of extending Newmark's approach to account for the change of slope geometry, or for shear strength reduction, or both.

Only a few of the models mentioned above account for both earthquake-induced shear strength reduction and changes in slope geometry and were validated against experimental data or well documented case-histories of landslides.

Also, in most of the proposed models internal shear surfaces at block boundaries are assumed, whose position is to be known *a priori*, or to be determined numerically with a considerable computational effort [28]. However, for landslides involving nearly homogeneous soil masses, these internal surfaces do not necessarily develop, most of the sliding occurring along the slip surface.

In this vein, a GLE-based model is presented, that permits to evaluate the earthquake-induced displacements of slopes accounting for sliding mechanisms of general shape and for both the stabilising effect induced by geometric rearrangement of soil mass during sliding and the weakening effect due to cyclic degradation of shear strength.

The model is based on the General Limit Equilibrium (GLE) method of analysis [29] that, differently from other classical methods of slices, satisfies full equilibrium providing a consistent estimate of stability conditions [2].

The sliding mass is divided into vertical slices along which shear strength is not necessarily fully mobilised, this implying that internal shear surfaces do not necessarily exist.

In the proposed model, the changes in slope geometry during sliding is evaluated according to Sarma and Chlimintzas [13] and shear strength reduction is described in terms of effective stresses, including pore water pressure build-up induced by cyclic loading, or in terms of total stresses, accounting for the reduction of undrained shear strength, using in both cases empirical relationships based on experimental results.

In the analysis, the critical acceleration of the slope is time dependent due to the changes induced by earthquake loading in slope geometry and soil shear strength. For each time step of the acceleration time history selected as input motion, critical acceleration is estimated, accounting for the current value of the soil shear strength and the deformed shape of the slope, by solving the pseudo-static limit equilibrium condition of the GLE method.

To evaluate the model capability in reproducing typical mechanisms of seismically induced deformations of natural slopes, the results of a series of shaking table tests carried out by Wartman et al. [30] on small scale model slopes are finally compared with model results in terms of cumulated permanent displacement and slope final configuration.

2. Proposed GLE-based model

According to Newmark [1], for a given acceleration time history, earthquake-induced displacements start whenever the seismic acceleration $a(t)=k_h(t)\bullet g$ exceeds the critical acceleration $a_c = k_c\bullet g$ (being g the gravity acceleration) and develop during the time intervals in which the relative velocity of the sliding mass is greater than zero.

The critical seismic coefficient k_c of a slope is related to its geometry and to the soil shear strength. If the changes in soil shear strength and in slope geometry during seismic motion are negligible, k_c can be assumed constant with time. Conversely, if one of the changes mentioned above is significant, k_c varies with time, decreasing with shear strength reduction and increasing, generally, with changes in slope geometry.

For each time step of the input motion, the proposed model alternates a pseudo-static analysis, to evaluate the current value of $k_c(t)$, and a displacement analysis, solving the differential equations of relative motion of the system.

In the pseudo-static analysis performed using the GLE method of slices the soil mass is divided into n vertical slices. In the displacement analysis the n slices are grouped into N blocks corresponding to the N straight-line segments describing the slip surface.

The displacement of each block along its base represents an independent degree of freedom of the system.

Four are the basic assumptions of the model: (i) each block slides along a different slip surface segment in a purely translational mode and the inter-block surfaces are, and remain, vertical during the motion; (ii) soil behaves as a perfectly plastic material obeying the Mohr–Coulomb failure criterion, in an effective stress (ES) analysis, and the Tresca failure criterion, in a total stress (TS) analysis; (iii) during sliding the shear strength along the slip surface is fully mobilized and is time dependent since pore pressure build-up and undrained shear strength reduction can be accounted for in ES and TS analyses, respectively; (iv) the critical acceleration is the same for all the blocks, this implying that the blocks start moving simultaneously and the shear strength is fully mobilized simultaneously along the slip surface.

2.1. Pseudo-static analysis using the GLE method of slices

The critical seismic coefficient of a slope is usually computed using the methods of slices assimilating the seismic action to an equivalent static force. The GLE method of slices is considered to

be rigorous since it makes the problem determinate and satisfies both force and moment equilibrium conditions. In this method a distribution of the inclination of the inter-slice forces within the sliding mass is defined through a function $f(x_i)$ and a scalar coefficient λ:

$$\frac{X_i}{E_i} = \lambda \times f(x_i) \tag{1}$$

In Eq. (1) x_i is the abscissa of the ith slice of the slope, $f(x_i)$ describes the variation of the inter-slice shear (X_i) and normal (E_i) forces across the slope; the coefficient λ represents the percentage of $f(x_i)$ used in the solution.

Fig. 1 shows the notations adopted in this paper.

Imposing horizontal force (f) and moment (m) pseudo-static equilibrium of the whole soil mass and solving for the slope safety factor, the following two equations can be derived:

$$F_f = \frac{\sum_{i=1}^{n} T_{i,\,\lim}}{\sum_{i=1}^{n} T_i} = \frac{\sum_{i=1}^{n} (c'_i \times l_i + N'_i \times \mathrm{tg}\varphi'_i) \times \cos\alpha_i}{\sum_{i=1}^{n} (N'_i + U_i) \times \sin\alpha_i + \sum_{i=1}^{n} k_h \times W_i} \tag{2}$$

$$F_m = \frac{\sum_{i=1}^{n} (c'_i \times l_i + N'_i \times \mathrm{tg}\varphi'_i) \times r_i}{\sum_{i=1}^{n} W_i \times (1 \pm k_v) \times h_i - \sum_{i=1}^{n} (N'_i + U_i) \times e_i + \sum_{i=1}^{n} k_h \times W_i \times v_i} \tag{3}$$

where c'_i and φ'_i are the effective cohesion and the angle of shearing resistance at the base of the ith slice, W_i is the slice weight, U_i is the resultant of the pore water pressure acting at the base of the ith slice, k_h and k_v are the horizontal and vertical components of the seismic coefficient, k_v being positive downwards, while the geometrical quantities α_i, e_i, r_i, l_i, h_i, v_i are shown in Fig. 1.

In Fredlund and Krahn [29], the normal effective forces N'_i acting at the base of the ith slice and the horizontal inter-slice force E_i acting between the ith and the $(i-1)$th slices can be obtained solving the local equilibrium equations in the vertical and horizontal directions; herein, local equilibrium parallel and normal to the base of the ith slice is considered:

$$N'_i = \frac{W_i \times (1 \pm k_v) + (X_{i-1} - X_i) - U_i \times \cos\alpha_i - \frac{c'_i \times l_i \times \sin\alpha_i}{F_{PS}}}{\cos\alpha_i + \frac{\sin\alpha_i \times \mathrm{tg}\varphi'_i}{F_{PS}}} \tag{4}$$

$$E_i = E_{i-1} + k_h \times W_i + (N'_i + U_i) \times \sin\alpha_i - \frac{c'_i \times l_i + N'_i \times \mathrm{tg}\varphi'_i}{F_{PS}} \times \cos\alpha_i \tag{5}$$

In Eqs. (4) and (5) F_{PS} is the pseudo-static safety factor of the slope. In the GLE method a value λ_{PS} is obtained that satisfies the condition $F_f = F_m = F_{PS}$ (Eqs. (2) and (3)).

In the proposed approach the GLE method was used to evaluate the horizontal component $k_{h,c}$ of the critical seismic coefficient k_c. In the analyses discussed in the next sections, the vertical component of the seismic acceleration is neglected since its effect on earthquake-induced permanent displacements is generally not relevant [31]. Thus, in the following the subscript 'h' is omitted in the notation and the symbols $k = a/g$ and $k_c = a_c/g$ are used for the horizontal seismic coefficient and its critical value.

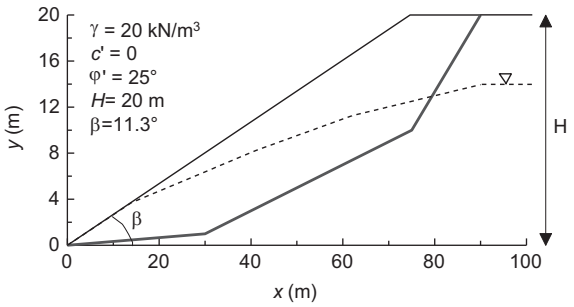

Fig. 2. Slope scheme adopted to validate the proposed algorithm.

Table 1
Comparison of results obtained through the proposed algorithm and *SLOPE/W v.5* [32].

	k_c	λ_c
Proposed algorithm	0.121	0.549
SLOPE/W	0.123	0.555
Relative error	1.62 %	1.08 %

Imposing the limit equilibrium condition $F_f = F_m = 1$, the expressions giving the corresponding values of $k_{c(f)}$ and $k_{c(m)}$ may be derived from Eqs. (2) and (3), respectively:

$$k_{c(f)} = \frac{\sum_{i=1}^{n} \frac{(c'_i \times l_i - U_i \times \mathrm{tg}\varphi'_i)}{\cos\alpha_i + \sin\alpha_i \times \mathrm{tg}\varphi'_i} - \sum_{i=1}^{n} (W_i + \Delta X_i) \times \mathrm{tg}(\alpha_i - \varphi'_i)}{\sum_{i=1}^{n} W_i} \tag{6}$$

$$k_{c(m)} = \frac{\sum_{i=1}^{n} (c'_i \times l_i - U_i \times \mathrm{tg}\varphi_i) \times (r_i \times \cos\alpha_i + e_i \times \sin\alpha_i / \cos\alpha_i + \sin\alpha_i \times \mathrm{tg}\varphi'_i) + \sum_{i=1}^{n} (((W_i + \Delta X_i) \times r_i \times \mathrm{tg}\varphi'_i - e_i)/(\cos\alpha_i + \sin\alpha_i \times \mathrm{tg}\varphi'_i)) - \sum_{i=1}^{n} W_i \times h_i}{\sum_{i=1}^{n} W_i \times v_i} \tag{7}$$

being $\Delta X = X_i - X_{i-1}$.

In a total stress analysis, Eqs. (2)–(5) with the condition $F_f = F_m = 1$ lead to

$$k_{c(f)} = \frac{\sum_{i=1}^{n} \left(\frac{(C_{u,i} \times l_i)}{\cos\alpha_i}\right) - \sum_{i=1}^{n} (W_i + \Delta X_i) n \mathrm{tg}\alpha_i}{\sum_{i=1}^{n} W_i} \tag{8}$$

$$k_{c(m)} = \frac{\sum_{i=1}^{n} C_{u,i} \times l_i \times (r_i + e_i \times \mathrm{tg}\alpha_i) - \sum_{i=1}^{n} \left(\frac{e_i}{\cos\alpha_i}\right) - \sum_{i=1}^{n} W_i \times h_i}{\sum_{i=1}^{n} W_i \times v_i} \tag{9}$$

where $C_{u,i}$ is the undrained shear strength at the base of the ith slice.

For each time step of the input motion selected for the displacement analysis, the current value of critical seismic coefficient $k_c(t)$ is found detecting the scalar coefficient λ_c (Eq. (1)) that

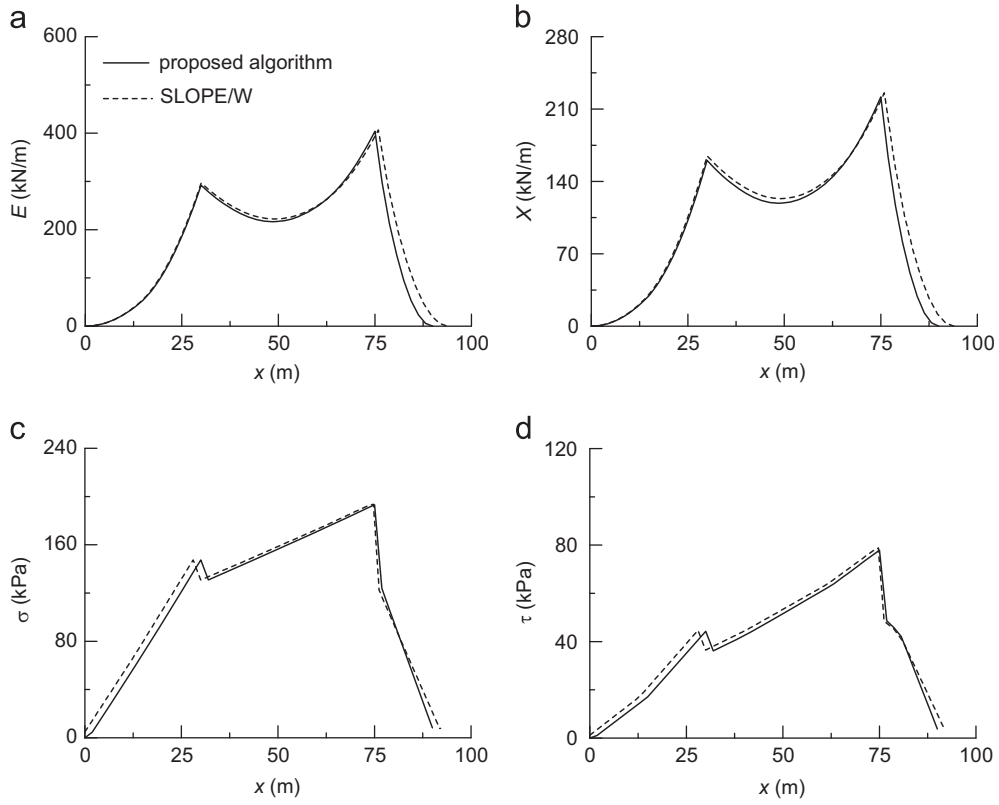

Fig. 3. Comparison of results obtained through the proposed algorithm and SLOPE/W: (a) normal and (b) shear inter-slice forces; (c) total normal and (d) shear stresses at the base of slices.

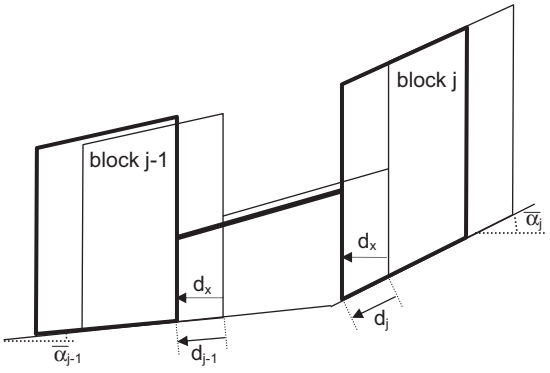

Fig. 4. Kinematic compatibility between two adjacent blocks during sliding.

satisfies both force (Eqs. (6) and (8)) and moment (Eqs. (7) and (9)) equilibrium, i.e.: $k_c = k_{c(f)} = k_{c(m)}$ for $\lambda = \lambda_c$.

The proposed GLE algorithm was implemented in a computer code. For its validation, different slope schemes were considered and the results were compared with those obtained, through an iterative procedure, by the commercial code *SLOPE/W v.5* ([32]). As an example, Fig. 2 shows a 20 m high slope with a slip surface consisting of three segments with different inclinations; the piezometric surface and the shear strength parameters are also shown in the figure. In the analyses the slope was divided into 90 slides. A very close agreement was obtained between the results provided by the two codes: differences in the values of k_c and λ_c were lower than 2% (Table 1); the distribution of inter-slice forces E_i and X_i and of normal and shear stresses along the slip surface resulted very close to each other (Fig. 3).

2.2. Displacement analysis

The slip mechanism assumed in the displacement analysis requires adjacent blocks, delimited by the straight-line segments describing the slip surface, to be rigidly connected to avoid any separation or overlapping at the contact of their bases with the slip surface and along the inter-block surfaces. The slip surface and the inter-block surfaces are assumed to remain fixed throughout sliding. Since the inter-block boundaries are assumed to be vertical, kinematic compatibility (i.e. no separation or overlapping with the slip surfaces and along block interfaces) implies that for two adjacent blocks $(j-1)$ and j, with base inclination $\overline{\alpha}_{j-1}$ and $\overline{\alpha}_j$, the horizontal components of displacements d_{j-1} and d_j coincide (Fig. 4):

$$d_x = d_{j-1} \times \cos\,\overline{\alpha}_{j-1} = d_j \times \cos\,\overline{\alpha}_j \tag{10}$$

For a system consisting of N blocks, the recursive use of Eq. (10) permits to express the displacement d_j of the jth block as a function of the displacement d_r of an arbitrary reference block by introducing a displacement conversion factor $q_{j,r}$:

$$d_j = d_r \times q_{j,r} \tag{11}$$

where

$$q_{j,r} = \begin{cases} \prod_{k=1}^{j-1} \dfrac{\cos\,\overline{\alpha}_k}{\cos\,\overline{\alpha}_{k+1}} & \text{if } j > r \\ 1 & \text{if } j = r \\ \prod_{k=1}^{j-1} \dfrac{\cos\,\overline{\alpha}_{k+1}}{\cos\,\overline{\alpha}_k} & \text{if } j < r \end{cases} \tag{12}$$

The equation of relative motion of the jth block of the slope is obtained by equating the unbalanced forces, acting parallel to the block base, to the inertial forces acting on the same block during

earthquake:

$$\overline{T}_j - \overline{T}_{j,\,\mathrm{lim}} = \frac{\overline{W}_j}{g} \times \ddot{d}_j(t) \tag{13}$$

In Eq. (13), $\overline{T}_j$ and $\overline{T}_{j,\,\mathrm{lim}}$ are the driving and the resisting shear forces acting at the base of the jth block, $\overline{W}_j$ is the block weight and $\ddot{d}_j(t)$ is the relative acceleration of the block with respect to the firm soil.

Using Eqs. (11) and (13), the equations of relative motion of all the blocks can be combined and the equation of relative motion of the reference block can be written as

$$\ddot{d}_r(t) = g \times \left[k(t) - k_c\right] \times S_r \tag{14}$$

where the shape factor S_r depends on the overall slope geometry (ground and slip surfaces) and on the shear strength mobilised at the base of the blocks:

$$S_r = \frac{\sum_{j=1}^{N}\left[\left(\prod_{k=1}^{N-1} A_k\right) \times \left(\prod_{k=j+1}^{N} B_k\right) \times (\overline{W}_j/\overline{W}_r) \times (\cos\overline{\alpha}_j + \sin\overline{\alpha}_j \times \mathrm{tg}\varphi'_j)\right]}{\sum_{j=1}^{N}\left[\left(\prod_{k=1}^{j-1} A_k\right) \times \left(\prod_{k=j+1}^{N} B_k\right) \times \left(\frac{\overline{W}_j}{\overline{W}_r}\right) \times q_{j,r}\right]} \tag{15}$$

$$S_r = \frac{\sum_{j=1}^{N}\left[\left(\prod_{k=1}^{j-1} A_{ko}\right) \times \left(\prod_{k=j+1}^{N} B_{ko}\right) \times \frac{\overline{W}_j}{\overline{W}_r} \times \cos\overline{\alpha}_j\right]}{\sum_{j=1}^{N}\left[\left(\prod_{k=1}^{j-1} A_{ko}\right) \times \left(\prod_{k=j+1}^{N} B_{ko}\right) \times \frac{\overline{W}_j}{\overline{W}_r} \times q_{j,r}\right]} \tag{16}$$

Eqs. (15) and (16) refer to an effective and a total stress analysis, respectively. In these equations $\overline{W}_r$is the weight of the reference block and

$$A_k = f(x_k) \times \lambda_c \times (\sin\overline{\alpha}_k - \cos\overline{\alpha}_k \times \mathrm{tg}\varphi'_k) + (\cos\overline{\alpha}_k + \sin\overline{\alpha}_k \times \mathrm{tg}\varphi'_k) \tag{17}$$

$$B_k = f(x_{k-1}) \times \lambda_c \times (\sin\overline{\alpha}_k - \cos\overline{\alpha}_k \times \mathrm{tg}\varphi'_k) + (\cos\overline{\alpha}_k + \sin\overline{\alpha}_k \times \mathrm{tg}\varphi'_k) \tag{18}$$

$$A_{ko} = f(x_k) \times \lambda_c \times \sin\overline{\alpha}_k + \cos\overline{\alpha}_k \tag{19}$$

$$B_{ko} = f(x_{k-1}) \times \lambda_c \times \sin\overline{\alpha}_k + \cos\overline{\alpha}_k \tag{20}$$

Neglecting the shape factor S_r, Eq. (14) coincides with the equation of relative motion of a single block having a critical seismic coefficient k_c and sliding on a horizontal plane when subjected to a horizontal acceleration time history $a(t) = k(t) \bullet g$, being $k(t)$ the current value of the horizontal seismic coefficient:

$$\ddot{d}_0(t) = g \times [k(t) - k_c] \tag{21}$$

Reduction of shear strength produced by seismic loading and rearrangement of slope geometry produced by earthquake-induced displacements can be taken into account introducing time dependent values of critical seismic coefficient $k_c(t)$ and of shape factor $S_r(t)$ of the slope.

The current value of $k_c(t)$ can be evaluated using Eqs. (6) and (7) or Eqs. (8) and (9) for an effective stress or a total stress analysis, respectively.

2.3. Shear strength reduction

In Eqs. (6) and (7) time dependent values of the resultant pore water pressure $U_i(t)$ are used, that account for pore water pressure build-up, while in Eqs. (8) and (9) the undrained shear strength $C_{u,i}(t)$ includes possible effects of shear strength reduction. In both cases, the time dependent value of the scalar coefficient $\lambda_c(t)$ corresponding to the condition $k_{c(f)}(t) = k_{c(m)}(t)$ is evaluated for each time step of analysis solving for horizontal force (f) and moment (m) limit equilibrium ($F_f = F_m = 1$). As a consequence, even though no change in slope geometry is considered in the analysis, Eqs. (15) and (16) provide a time dependent value of $S_r(t)$ through the scalar coefficient $\lambda_c(t)$ included in Eqs. (17)–(20).

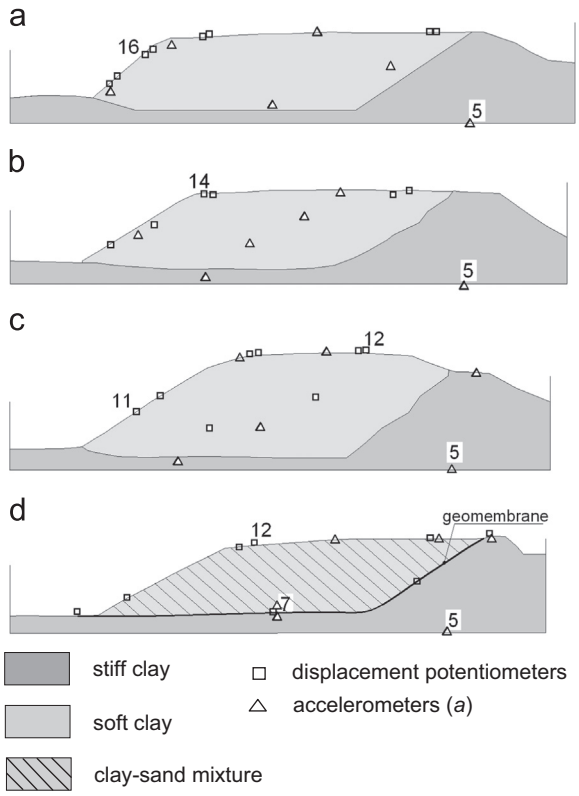

Fig. 6. Model slopes: geometry and instruments location (adapted from Wartman et al. [30]).

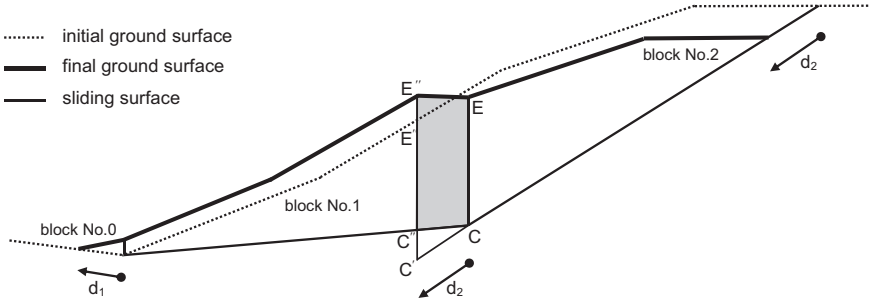

Fig. 5. Rearrangement of ground surface during sliding and introduction of "block No. 0" at the toe of the slope.

Bandini [27] and Bandini et al. [20] proposed procedures for the evaluation of time dependent values of $U_i(t)$ and $C_{u,i}(t)$ for an effective or total stress analysis, respectively. Herein the main aspects of these procedures are summarized with reference to fine-grained soils only, focusing on the evaluation of undrained shear strength which is adopted in this paper for the validation of the proposed model.

When subjected to cyclic loading, saturated fine-grained soils may experience a strength reduction that is related to both cyclic degradation and pore pressure build-up (e.g. [33,34]). This reduction occurs when the cyclic shear strain $\gamma_c(t)$ overcomes a volumetric threshold γ_v which depends on some intrinsic soil characteristics, usually related to the plasticity index PI, and on the overconsolidation ratio (e.g. [35]).

In the procedure proposed for effective stress analyses, the excess pore water pressure ratio $\Delta u^* = \Delta u/\sigma'_{n0}$ induced at the base of the ith slice after the jth significant straining cycle ($N_{i,j}$) can be evaluated as the product of its maximum value $\Delta u^*_{i,max}$ and a weighting factor $\varepsilon_{i,j}$:

$$\Delta u^*_{i,j} = \Delta u^*_{i,\,max} \times \varepsilon_{i,j} = \Delta u^*_{i,\,max} \times \frac{\log\left(\gamma_{m,i}/\gamma_v\right)_j}{\sum_{s=1}^{N_{i,j}} \log\left(\gamma_{m,i}/\gamma_v\right)_s} \tag{22}$$

Table 2
Model properties and initial values of critical seismic coefficient.

Slope	*H* (cm)	Upper soil layer						$k^*_{c,p}$	$k_{c,r}$
		$C_{u,p}$ (kPa)	$C^*_{u,p}$ (kPa)	$C_{u,r}$ (kPa)	δ	Geomembrane interface φ^* (°)	c_a (kPa)		
1	16.7	2.20	2.75	1.58	0.07	–	–	2.12	1.12
2	18.7	2.34	2.94	1.55	0.10	–	–	1.63	0.79
3	26.5	2.68	3.21	1.77	0.10 0.18	–	–	1.35	0.64
4	20.1	–	–	–		22.1°	0.9	0.26	–

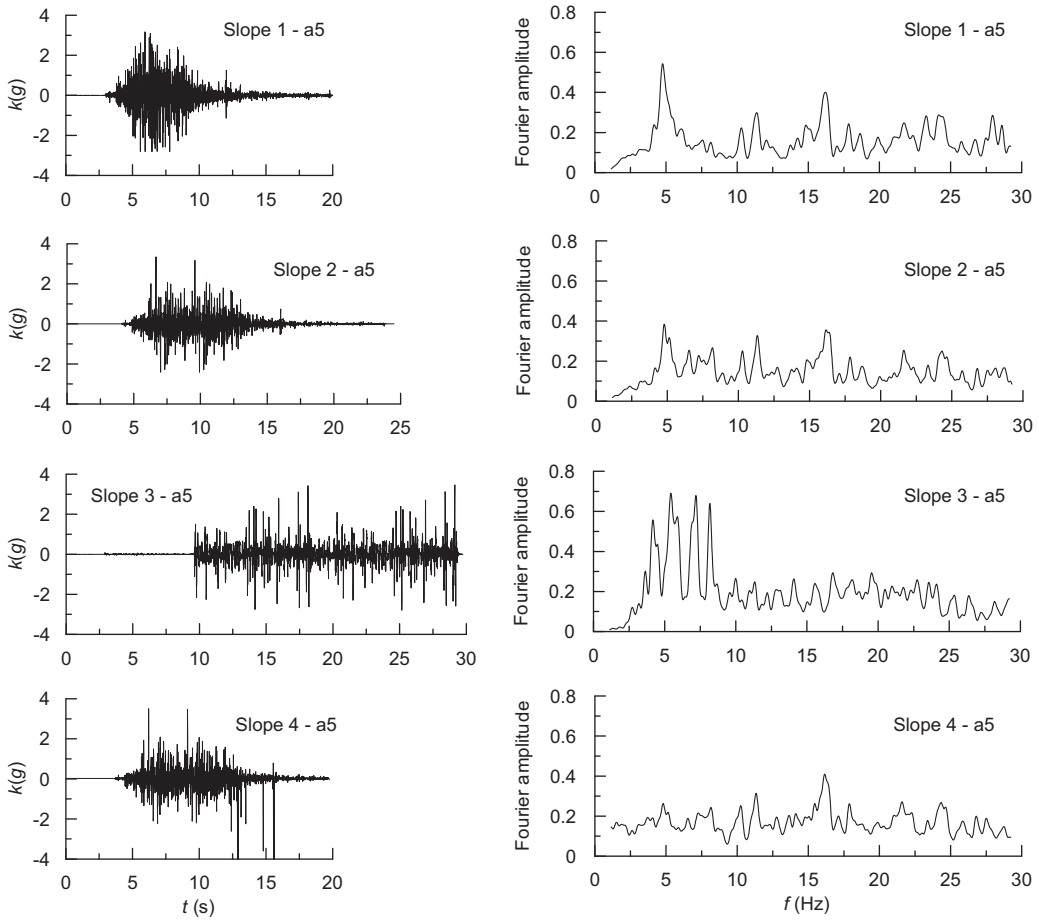

Fig. 7. Acceleration time histories recorded by accelerometer *a*5 on the shaking table and corresponding smoothed Fourier amplitude spectra.

Table 3
Motion characteristics recorded by accelerometers *a*5 on the shaking table.

Slope	Test motion	PGA (g)	Arias intensity I_a (m/s)	Significant duration [44] D (s)	Mean period [45] T_m (s)	Destructiveness potential factor [46] P_d (g/s^3)	Equivalent number of cycles [40,41] N_{eq}
1	Modified Kobe Port Island	3.17	66.42	4.93	0.13	18.5	93
2	Modified Kobe Port Island	3.35	40.36	6.54	0.12	16.8	27
3	Synthetic	3.46	95.52	18.51	0.15	74.6	54
4		4.00	51.47	9.46	0.19	24.1	–

Table 3 (*continued*)

The expression for factor $\varepsilon_{i,j}$ in Eq. (22) was derived starting from the model of pore water pressure generation proposed by Matsui et al. [33] and assuming that the pore pressure build-up can be distributed over the number of significant cycles $N_{i,j}$ according to Miner's law of cumulative damage. In the same equation, $\gamma_{m,i}$ represents the average cyclic amplitude for the ith slice and is defined as the mean value between the positive and negative peaks in the jth straining cycle. Eq. (22) applies only for significant cycles ($N_{i,j}$) for which $\gamma_{m,i} > \gamma_v$, thus requiring the evaluation of the $\gamma_{c,i}$ time history for each slice. Due to the generality of the proposed procedure, any other model of pore water pressure generation proposed in the literature can be used to estimate $\Delta u^*_{i,max}$ and the weighting factor $\varepsilon_{i,j}$.

In the procedure proposed for a total stress analysis, the shear strength reduction is evaluated introducing the degradation parameter δ ([36]):

$$\frac{C_u(N_{i,j})}{C_{u,0}} = N_{i,j}^{-\delta} \tag{23}$$

where $C_u(N_{i,j})$ is the undrained shear strength available at the base of the ith slice after the jth significant straining cycles $N_{i,j}$ and $C_{u,0}$ is its initial value.

The degradation parameter δ depends on the amplitude $\gamma_c(t)$ of the earthquake-induced shear strain and on the volumetric threshold shear strain γ_v. According to Ishihara [37], values of δ in the range of 0.07–0.25 are representative of the cyclic behaviour of normally consolidated clays for shear strain amplitudes varying from 0.3 to 2.4%.

Depending on the analyses to be carried out (ES or TS analyses), the significant straining cycles $N_{i,j}$ can be evaluated using the time history of the earthquake-induced shear-stress, $\Delta\tau_{c,i}(t)$, or, alternatively, the time history of the corresponding shear-strain, $\gamma_{c,i}(t)$ at the base of the ith slice; the latter is required in any case to compute $\gamma_{m,i}$ and to check the condition $\gamma_{m,i} > \gamma_v$.

In the proposed approach $\Delta\tau_{c,i}(t)$ is evaluated from the driving shear forces T_i computed at the base of the ith slice, for each time step of a given acceleration time history; $N_{i,j}$ is evaluated using established procedures for converting an irregular time history of shear stress into an equivalent uniform time history (e.g. [38–41]), thus computing the number of equivalent loading cycles.

Starting from $\Delta\tau_{c,i}(t)$, the time history $\gamma_{c,i}(t)$ of the shear strain induced at the base of the ith slice is computed solving iteratively

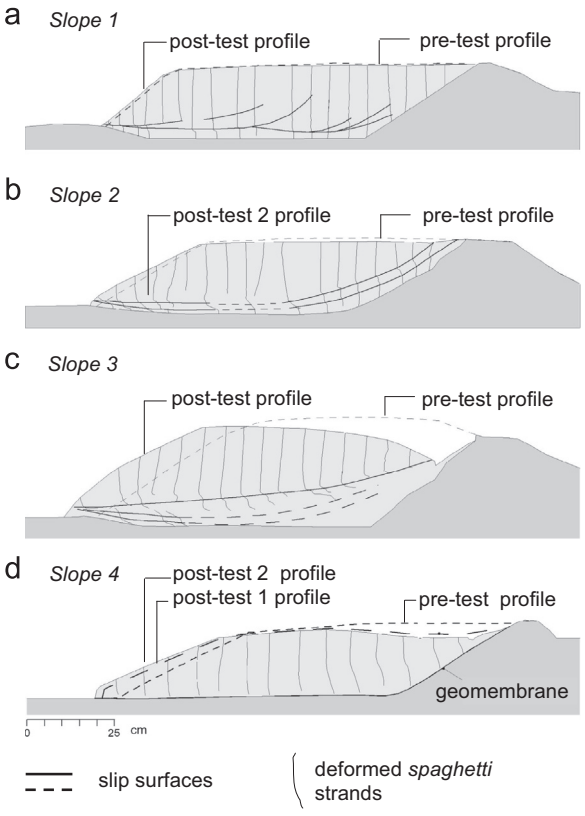

Fig. 8. Model slopes: pre-test and post-test slope profiles (adapted from Wartman et al. [30]).

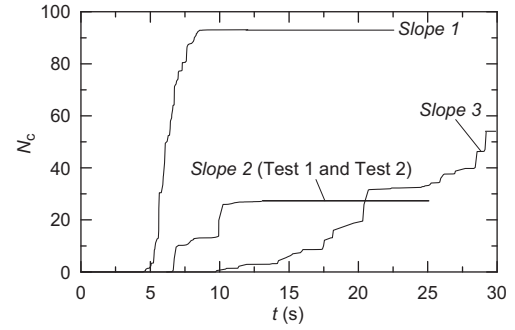

Fig. 9. Time-histories of the number of loading cycles.

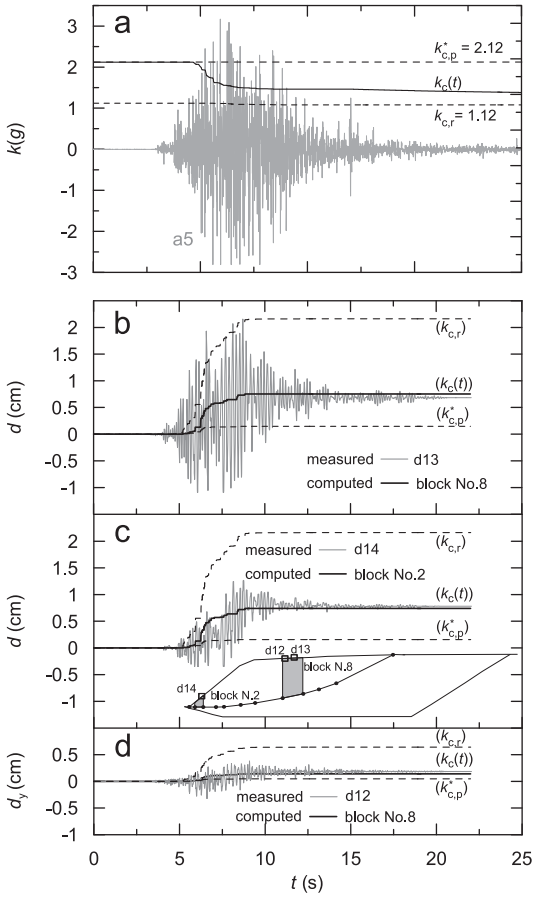

Fig. 10. *Slope* 1: (a) acceleration time histories of base input motion $k(t)$ and values of critical seismic coefficient; (b)–(d) measured (d12–13–14) and computed (block No. 2 and 8) displacements.

the following equation:

$$\gamma_{c,i}(t) = \frac{\frac{0.65 \times \Delta\tau_{c,i}(t)}{G_{0,i}}}{\frac{G(\gamma_{c,i})}{G_{0,i}}} \quad (24)$$

where $G_{0,i}$ is the small strain shear modulus at the base of the ith slice and $G(\gamma_{c,i})/G_{0,i}$ describes the reduction of normalized shear modulus with the induced strain level.

It is worth noting that the proposed procedure permits to use either the experimental values or given empirical relationships for the small strain shear modulus G_0 and its reduction with the induced strain level.

Once $\gamma_{c,i}(t)$ is estimated, those cycles for which the mean cyclic amplitude $\gamma_{m,i}$ is greater than the volumetric threshold γ_v can be detected and, as a consequence, the time history of significant straining cycles $N_{i,j}$ is obtained.

2.4. Mass transfer

To describe the rearrangement of slope geometry during sliding, the weight $W_i(t)$ of the ith slice must be updated at each time step of analysis modifying the geometric configuration of the ground surface. Accordingly, the geometric parameters (e_i, r_i, l_i, h_i and v_i) involved in Eqs. (2)–(9) are updated and the weight $\overline{W}_j$ of the jth block is changed as well. Then, current values of $\lambda_c(t)$ and of $k_c(t)$ are computed at each time step of motion through Eqs. (6)–(9) and a time dependent value of $S_r(t)$ is computed through Eqs. (15) and (16). In this case, even though no strength reduction is considered in the analysis, time dependent values of $k_c(t)$ and $S_r(t)$ are obtained as a consequence of the change in the slice (W_i) and block ($\overline{W}_j$) weights.

When reduction of shear strength and changes in slope geometry are both accounted for in the displacement analysis, the critical seismic coefficient $k_c(t)$ and the shape factor $S_r(t)$ depend on current values of $U_i(t)$ or $C_{u,i}(t)$ and on computed time histories of $W_i(t)$, $\overline{W}_j(t)$and $\lambda_c(t)$.

To satisfy kinematic compatibility of block displacements, the rearrangement in slope geometry requires that part of the mass of a block is transferred into the adjacent block during motion. Since the slip surface and the inter-block surfaces are assumed to remain unchanged throughout the displacement analysis, the deformed slope geometry is fully defined by the deformed shape of the ground surface; at each time step, this is computed applying the principle of mass conservation at all the internal shear surfaces as displacements develop. The larger is the number of straight-line segments considered in the analysis to describe the slip surface (i.e. the larger is the number of considered blocks), the more accurate is the prediction of the final configuration of the ground surface.

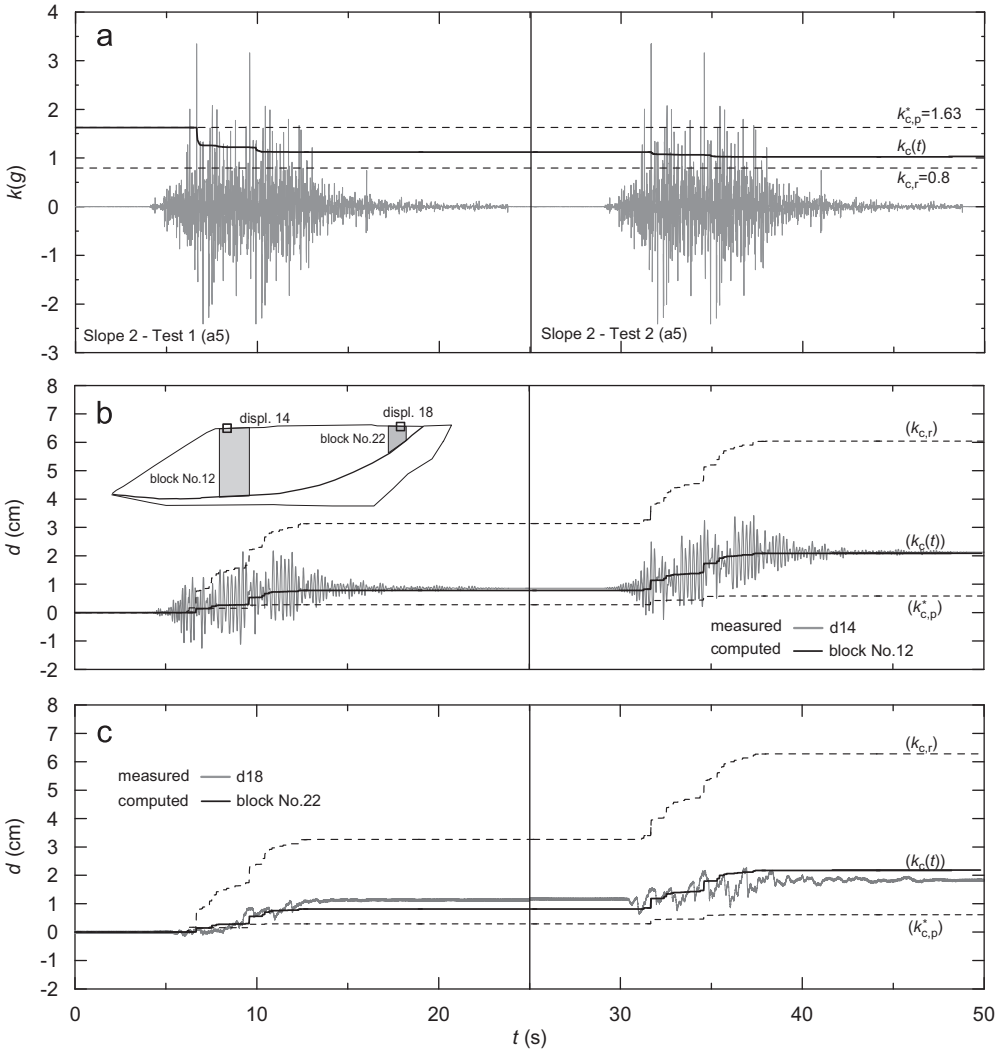

Fig. 11. Test 1 and 2 on *Slope* 2: (a) acceleration time histories of base input motion $k(t)$ and values of critical seismic coefficient; (b and c) measured ($d14$–$d18$) and computed (blocks No.12 and 22) displacements.

Fig. 5 shows the mechanism of mass transfer and geometry change for a simple two-segment slip surface (i.e. two-block system). The mass enclosed in $CC'C''$, associated to displacement of block No. 2, cannot cross the sliding surface thus it is transferred into block No.1; moreover, in the updated slope configuration the mass enclosed in the area $CC'E'E$ is equal to that enclosed in the area $CC''E''E$.

Mass transfer from one block to another, and the consequent transition towards a more stable slope configuration, depends substantially on the possibility of accumulating a soil mass at the toe of the slope; a fictitious block (block No. 0 in Fig. 5) is then introduced in the model at the toe of the slope; at the beginning of the analysis the sliding surface and the ground surface of the fictitious block coincide to reproduce the initial condition of no weight ($\overline{W}_0 = 0$ for $t=0$). During sliding, as a result of application of the principle of mass conservation to the two blocks, the weight of the fictitious block No. 0 increases due to mass transfer from block No. 1 and the ground surface changes accordingly.

When permanent displacements induced by earthquake loading are large, changes in slope geometry become significant and should be considered for a reliable evaluation of its seismic performance. Conversely, mass transfer effects can be neglected, assuming the blocks to behave as rigid bodies, when earthquake-induced displacements are small if compared to the slope dimensions. In this latter case, if shear strength degradation can also be disregarded, k_c (Eqs. (6)–(7) (or 8)–(9)) and S_r (Eqs. (15) and (16)) are constant with time and Eq. (14) can be written as

$$\ddot{d}_j(t) = S_r \times \ddot{d}_0(t) \tag{25}$$

Then, using Eq. (11), the displacement of jth block of the system is:

$$d_j(t) = S_r \times q_{j,r} \times d_0(t) \tag{26}$$

where $d_0(t)$ is the time history of the permanent displacement of an ideal rigid block, having the same critical acceleration of the slope and sliding on a horizontal plane; $d_0(t)$ can be evaluated integrating twice Eq. (21).

3. Validation of the proposed model

To verify the capability of the proposed model to reproduce the deformation patterns induced by seismic events, a series of shaking table tests carried out by Wartman et al. [30] on small-scale model slopes were back-analysed.

The tests were performed on four clayey slope models (*Slope1*, *Slope 2*, *Slope 3* and *Slope 4*) constructed in a rigid box container and instrumented with solid piezo-resistive accelerometers and linear motion potentiometers. Uncooked *spaghetti* strands, pushed vertically into the slope models at regular spacing, were used as inclinometers.

The clayey slope models consisted of an upper layer of soft clay ($w=128.1\%$; $PI=106$ %) underlain by a stiffer clay ($w=115\%$, $PI=106\%$) introduced to minimise the influence of the container boundaries on the models behaviour.

The geometry and the instrumentation of the four model slopes are shown in Fig. 6 at the model scale; Table 2 summarizes peak ($C_{u,p}$) and remoulded ($C_{u,r}$) values of the undrained shear strength, measured using a portable laboratory-scale vane shear. Wartman et al. [30] showed that peak undrained shear strength of the clay used in the tests on model *Slope* 1–3 is affected by strain rate effect leading to an increase of 10% to 20% ($C^*_{u,p}$ in Table 2) with respect to the measured peak values ($C_{u,p}$ in Table 2).

In model *Slope* 4, two sheets of smooth HDPE geomembranes were placed above the layer of stiff clay to induce strain localisation along the geomembrane-geomembrane interface and a clay–sand mixture was used for the upper layer to increase the unit weight and, thus, the driving stresses.

According to Kim et al. [42], Wartman et al. [30] adopted an interface friction angle $\varphi^*=22.1^\circ$ at the contact between the geomembranes.

The input motions used in the tests on *Slope* 1, *Slope* 2 and *Slope* 4 consisted of differently scaled and time compressed records of the 1995 Hyogoken-Nanbu earthquake; two identical input motions were applied in close succession to *Slope* 2 to study the model response along pre-existing sliding surfaces. For *Slope* 3, a synthetic input motion was intentionally created with higher energy content.

Fig. 7 shows the acceleration time histories recorded by accelerometers *a5* installed on the shaking table and the

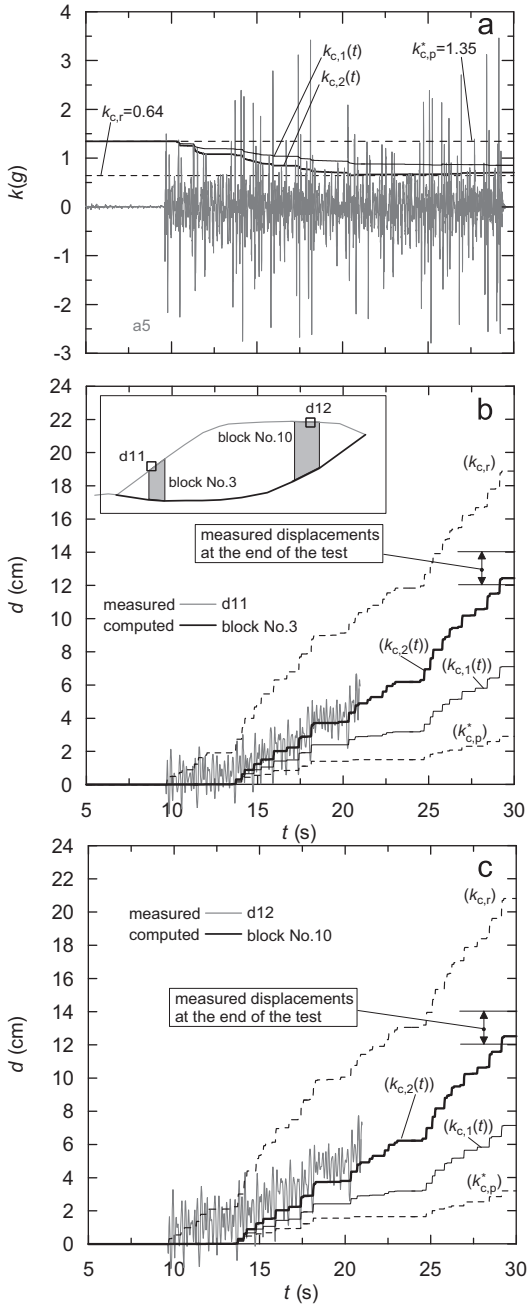

Fig. 12. *Slope* 3: (a) acceleration time histories of base input motion $k(t)$ and values of critical seismic coefficient; (b) measured ($d11$–$d12$) and computed (blocks No.3 and10) displacements.

corresponding smoothed Fourier amplitude spectra. The main characteristics of the input motions are listed in Table 3; records adopted for *Slopes* 1, 2 and 4 have quite comparable values of destructiveness potential factor P_d and significant duration D_s whereas the synthetic motion (*Slope* 3) is characterized by much larger values of Arias intensity I_a, P_d and D_s.

The pre- and post-test profiles of model slopes are shown in Fig. 8 together with the shear surfaces detected at the end of the tests. Vertical lines in the soft clay layer represent the position of the deformed *spaghetti* strands.

3.1. Model simulations

The observed slope responses were reproduced through the proposed model using the acceleration time histories recorded by accelerometer *a5*, installed on the shaking table, as input motions. In the analyses, the observed sliding surfaces were approximated with straight-line segments thus dividing the sliding mass into *N* rigid blocks; a fictitious block No. 0 was introduced at the toe of each slope.

Total stress displacement analyses were carried out for *Slopes* 1–3 assuming either corrected peak values of undrained strength ($C^*_{u,p}$), to account for strain rate effects, or remoulded values of undrained shear strength ($C_{u,r}$), attained at large strains, taking into account for both shear strength reduction and mass transfer. Conversely, effective stress analyses were carried out to back-analyse model test on *Slope* 4, in which sliding was forced at the contact between the geomembranes, characterised by an interface friction angle $\varphi^*=22.1^\circ$ (Table 2); mass transfer only was then accounted for in this analysis to evaluate the critical seismic coefficient.

In the analysis, for *Slope* 1–3 the undrained shear strength $C_u(N_c)$ available after a number N_c of loading cycles was evaluated using Eq. (23). The number of loading cycles N_c was computed according to Biondi et al. [40,41], through a conversion procedure in which all the cycles of the input motion were detected, properly normalized, and weighted using a conversion curve derived from the experimental data obtained by Idriss and Boulanger [43] for clayey and clay-like soils.

In the analyses $C_{u,0}=C^*_{u,p}$ was assumed and proper values of δ were detected through a back analysis of the experimental data. Specifically, $\delta=0.07$ and 0.10 were adopted for *Slope* 1 and 2, respectively, and $\delta=0.10$ and 0.18 were used for *Slope* 3. These values are consistent with the average degradation parameter $\delta=0.135$ that describes the conversion curve derived from the data by Idriss and Boulanger [43]; furthermore, values of $\delta=0.07$ and 0.18 fall within the range ($\delta=0.07/0.24$) suggested by Ishihara [37] for normally consolidated clay, for values of $\gamma_c=0.3/2.4\%$.

Time histories of N_c computed for *Slopes* 1–3 are shown in Fig. 9; N_c values increase suddenly at about 5–7s for the test

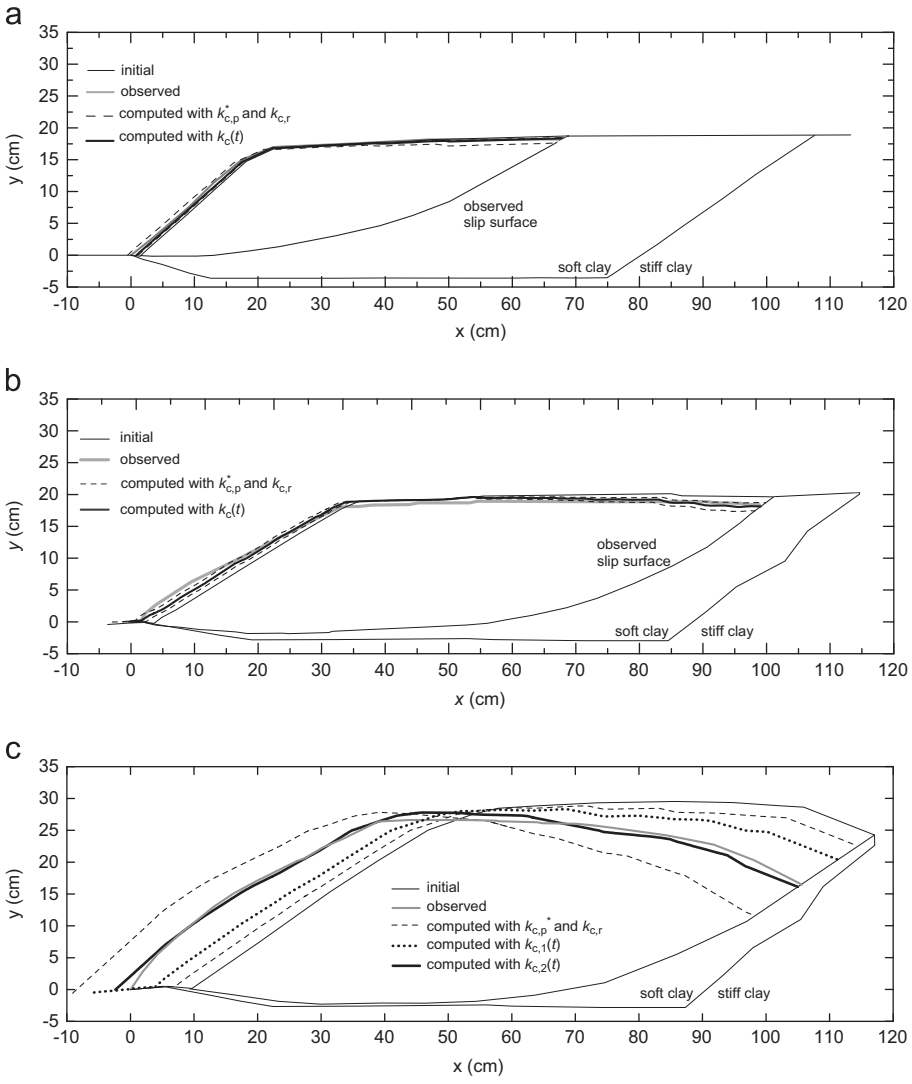

Fig. 13. Comparison between observed and computed ground surface of model slopes at the end of shaking.

motions of *Slopes* 1–2 while increases throughout the whole acceleration time history for the synthetic motion used for *Slope* 3, consistently with the shape of the accelerograms. The cumulative values N_{eq} of N_c are listed in Table 3.

Results of the displacement analyses for *Slopes* 1–3 are shown in Figs. 10–14. Table 4 reports the correspondence between the displacements of the model slopes measured by the potentiometers and the block displacements computed in the analyses.

In Figs. 10a, 11a and 12a the input acceleration time history $k(t)$ is superimposed to the critical seismic coefficients, $k^*_{c,p}$, $k_{c,r}$ and $k_c(t)$, evaluated assuming a constant value $C^*_{u,p}$ of peak undrained strength (corrected to account for strain rate effects), a constant value $C_{u,r}$ of remoulded undrained strength attained at large strains, and, finally, a time dependent value of $C_u(t)$, that accounts for shear strength reduction.

During the test on model *Slope* 3, slope deformations exceeded the range of the potentiometers so that only the initial portion of the displacement time histories were recorded; specifically, after 21 seconds of dynamic excitation the maximum displacement was equal to about 6 cm (Fig. 12b and c). Wartman et al. [30] supplemented the potentiometer measurements with those obtained from the survey targets installed on the model surface, evaluating final displacements in the range of 12–14 cm.

The analysis results (Figs. 10–12) show that the measured final displacements cannot be reproduced satisfactorily if a constant value of undrained shear strength, either measured at peak and corrected for strain rate effects ($C^*_{u,p}$) or the remoulded value attained at large strains ($C_{u,r}$), is used. In fact, the displacement time histories computed in these hypotheses, shown by dashed lines in Figs. 10–12, respectively represent, in all cases, a lower and an upper bound to the displacements measured during shaking. Vice versa, if time dependent values of $k_c(t)$ are computed accounting for the reduction of undrained strength, a good agreement is obtained between observed and computed displacements of the model slopes, both in terms of displacement time histories and of maximum permanent displacement at the end of shaking.

Specifically, experimental results of models *Slope* 1 (Fig. 10b–d) and *Slope* 2 (Fig. 11b and c) were reproduced with a good accuracy using values of the degradation parameter $\delta=0.07$ and 0.10 in Eq. (23), respectively. For *Slope* 1, the agreement holds for both displacements d, computed parallel to the base of the blocks, and its vertical component d_y. For *Slope* 2, model computations match the average trend of the whole slope response (*Test* 1 and *Test* 2) and the displacements cumulated at the end of *Test* 2.

The synthetic input motion applied to *Slope* 3 was much more severe than the records used for *Slopes* 1 and *Slope* 2; values of Arias Intensity I_a were in fact 1.4 to 2.4 times higher, while values of

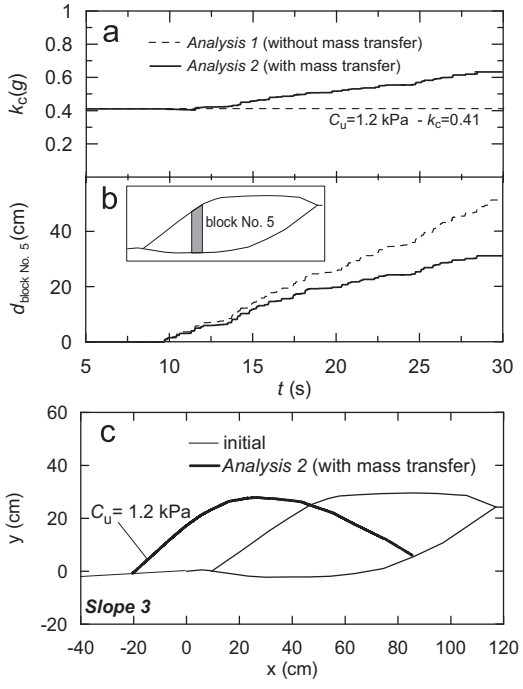

Fig. 14. Effect of mass transfer on permanent displacements computed for model *Slope* 3.

Table 4
Correspondence between measured (potentiometer) and computed (block) displacements and relevant figures.

Slope	Potentiometer	Block no.	Figure
1	*d*13	8	(10)b
	*d*14	2	(10)c
	*d*12 (vertical)	8 (vertical)	(10)d
2	*d*14	12	(11)b
	*d*18		(11)c
3	*d*11	322	(12)b
	*d*12	10	(12)c
4	*d*12	2	(15)b
	*d*18	7	(15)c

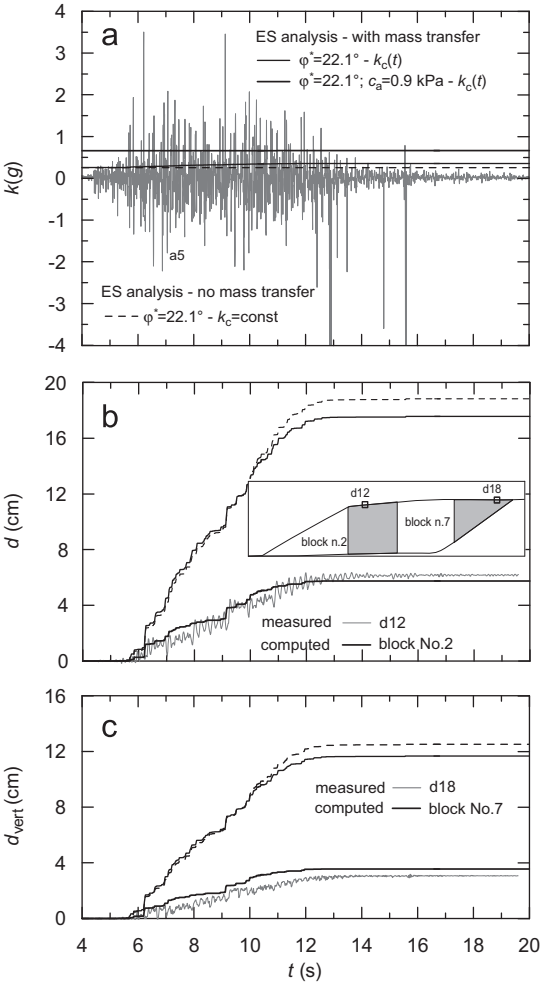

Fig. 15. *Slope* 4: (a) acceleration time histories of base input motion $k(t)$ and values of critical seismic coefficient; (b) measured (*d*12–*d*18) and computed (blocks No.2 and 7) displacements.

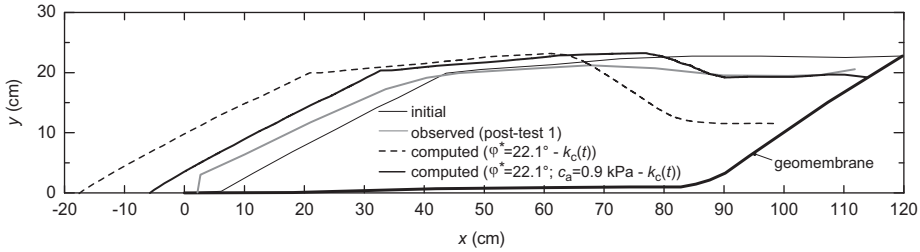

Fig. 16. *Slope* 4: comparison between observed and computed ground surface of model slope at the end of the shaking.

destructiveness potential factor P_d were about 4 times larger than the corresponding values of the records used for *Slopes* 1–2 (Table 3). As a consequence, a greater reduction of undrained shear strength may be envisaged for *Slope* 3. Accordingly, both $\delta=0.10$ ($k_{c,1}(t)$) and $\delta=0.18$ ($k_{c,2}(t)$) were used in the analysis. As shown in Fig. 12 the latter value led to a fair agreement with the displacements measured by the potentiometers $d11$ and $d12$, up to 21 s, and by the survey targets, at the end of shaking (Fig. 12b and c).

In addition to the cyclic degradation of undrained shear strength, the analyses accounted for the mass transfer between adjacent blocks, thus reproducing the ground surface profiles at the end of the tests. Fig. 13 compares the observed and the computed ground surface profiles for *Slope* 1–3; dashed lines refer to results obtained assuming a constant undrained shear strength ($C^*_{u,p}$ or $C_{u,r}$), while thick full lines are for computations performed using time dependent values of $C_u(t)$. Consistently with displacement computations, constant values of undrained shear strength provides lower and upper bounds to the observed slope profiles at the end of shaking, while slope geometry is described satisfactorily when accounting for the undrained strength reduction through the degradation parameter δ.

In general, the influence of shear strength reduction prevails when large permanent displacements occur, as in the case of *Slope* 3 (Fig.13c). The decreasing trend of the critical acceleration $k_c(t)=a_c(t)/g$ computed for all the slopes (Figs. 10a, 11a, 12a), implies that rearrangement of slopes geometry did not produce a significant stabilising effect during sliding, while shear strength reduction ruled the seismic slope response. This result can be attributed to the values of permanent displacements which were small if compared with slope dimensions.

To isolate and evaluate the effect of the mass transfer on the predicted final displacement of a slope, two displacement analyses (*Analysis* 1 and 2) were carried out using the geometry of *Slope* 3, but assuming a constant small value of undrained shear strength ($C_u=1.2$ kPa) to induce large permanent displacements during shaking.

Fig. 14 shows the results of these analyses. In *Analysis* 1, in which no mass transfer was taken into account, a constant value of the critical seismic coefficient $k_c=0.41$ was evaluated and a permanent displacement of about 51 cm was computed for block No.5 (Fig. 14a and b). In this hypothesis (no mass transfer) it is not possible to draw any deformed ground profile. In *Analysis* 2 the mass transfer is described and the critical acceleration increases as a results of the stabilising effect induced by changes in slope geometry (Fig. 14a), with a permanent final displacement $d=31$ cm (Fig. 14b) reduced of about 40% with respect to the case of *Analysis* 1. Fig. 14c also shows that, in addition to a reduction in the permanent slope displacements, the mass transfer also produces significant changes in the slope ground profile.

In model *Slope* 4, sliding was forced at the contact between the two geomembranes installed above the lower layer of stiff clay representing the firm soil (Fig. 8d); accordingly, its seismic behaviour was simulated through an effective stress analysis in which no reduction of shear strength was taken into account. It is worth noting that Wartman et al. [30] carried out two tests on *Slope* 4, while results from the first test only are back-analysed herein.

The displacement analyses were carried out assuming different values of the strength parameters at the geomembranes interface, either accounting or not for the effect of mass transfer.

The analysis results are shown in Fig. 15; again, Table 4 reports the correspondence between potentiometer and block displacements.

Assuming $\varphi^*=22.1^\circ$, as suggested by Wartman et al. [47], the analyses overestimated the observed displacements regardless the stabilising effect due to rearrangement of slope geometry. In fact, final permanent displacements in the range of 17–19 cm were computed for block N. 2 accounting for or neglecting the mass transfer effect, whereas the displacement measured at the end of the test by potentiometer $d12$ was equal to about 6 cm (Fig. 15b). Similarly, the vertical displacement of block No.7 ($d_y=12$ cm) resulted much higher than the vertical displacement measured by potentiometer $d18$ (Fig. 15c).

Following the experimental results by Kim [48], the shear strength at the contact between two geomembranes can be described using a Mohr–Coulomb failure criterion with a friction angle $\varphi^*$and an apparent cohesion c_a which, for the low stress level of the problem at hand, can be assumed to be in the range of 0.6–1 kPa.

The results of the analysis performed assuming $c_a=0.9$ kPa and $\varphi^*=22.1^\circ$ and accounting for the mass transfer effect show that the critical seismic coefficient slightly increases from $k_c(t)=0.64$ to $k_c(t)=0.66$ (Fig. 15a) with values of computed permanent displacement d for block No. 2 (Fig. 15b) and of displacement d_y for block No. 7 (Fig. 15c) that matches satisfactorily the corresponding measured displacements.

The comparison between the computed and the observed ground surface profiles at the end of shaking is shown in Fig. 16; if an apparent cohesion is assumed at the geomembranes interface, the results of the analysis are seen to be in a fair agreement with the observed ground surface profile of the model slope.

4. Concluding remarks

In this paper, a GLE-based model is presented to evaluate the permanent slope displacements induced by seismic loading.

The model permits to account for the stabilising effect associated to changes in slope geometry that occurs as displacements develop, and for the weakening effect induced by shear strength reduction that is possibly induced by earthquake loading. Changes in slope geometry are taken into account imposing the kinematic compatibility of block displacements and applying the principle of mass conservation at all the inter-block surfaces. Shear strength reduction can be simulated in both effective stress analyses, evaluating the pore water pressure build-up, and total stress analyses, estimating the progressive reduction of undrained shear strength.

In both cases, time dependent values of the critical seismic coefficient of the slope are evaluated applying the General Limit Equilibrium Method which was implemented in the model and checked against a reliable commercial code for slope stability analysis.

Differently from most of existing multi-block models, in the proposed GLE-based model the occurrence of slope displacements does not necessary require the full mobilisation of shear strength along surfaces internal to the soil mass involved in the failure mechanism. Thus, the proposed model is suitable to describe also seismic-induced landslides involving nearly homogeneous soil masses, in which sliding occurs mainly along the slip surface.

The capability of the proposed model to capture the main features of the seismic response of slopes was validated through effective stress and total stress back-analyses of a series of shaking table tests performed on small-scale model slopes made of clayey soils.

The observed and computed slope behaviours were compared in terms of displacement time histories at given locations in the slope models and in terms of deformed slope geometry at the end of shaking.

All the analyses provided a satisfactory estimate of the observed seismic performance of the model slopes if the shear strength reduction and/or the mass transfer effects were properly taken into account.

The agreement obtained between the observed and computed response of the model slopes suggests that the proposed model may be considered as a promising tool to evaluate the seismic performance of natural slopes expressed in terms of earthquake-induced permanent displacements and of ground surface deformations.

Acknowledgements

Prof. J. Wartman is gratefully acknowledged for having provided the experimental data on the shaking table tests carried out on small scale model slopes. The Authors wish also to thank the ReLUIS (University Network of Seismic Engineering Laboratories) Consortium which funded the research project on seismic slope stability.

References

[1] Newmark NM. Effect of earthquakes on dams and embankments. The Rankine lecture. Geotèchnique 1965;15(2):139–60.
[2] Bray JD. Simplified seismic slope displacement procedures. In: Pitilakis KD, editor. Earthquake geotechnical engineering. Springer; 2007. p. 327–53.
[3] Lemos L.J.L., Gama A.M.P., Coelho PALF. Displacement of cohesive slopes induced by earthquakes loading. In: Proceedings of the 13th international conference on soil mechanics and foundation engineering, New Delhi; 1994.
[4] Tika-Vassilikos TE, Sarma SK, Ambraseys N. Seismic displacements on shear surfaces in cohesive soils. Earthquake Eng Struct Dyn 1993;22:709–21.
[5] Sarma SK. Seismic stability of earth dam and embankments. Geotèchnique 1975;25(4):743–61.
[6] Biondi G, Cascone E, Maugeri M, Motta E. Seismic response of saturated cohesionless slopes. Soil Dyn Earthquake Eng 2000;20(1-4):209–15.
[7] Biondi G, Cascone E, Maugeri M. Flow and deformation failure of sandy slopes. Soil Dyn Earthquake Eng 2002;22(9-12):1104 (-1014).
[8] Gerolymos N, Gazetas G. A model for grain-crushing-induced landslides application to Nikawa, Kobe 1995. Soil Dyn Earthquake Eng 2007;27:803–17.
[9] Stamatopoulos C. Analysis of a slide parallel to the slope. In: Proceedings og the second Greek national conference of geotechnical engineering, vol. 1: p. 481–488 (in Greek), 1992.
[10] Ambraseys N, Srbulov M. Earthquakes induced displacement of slopes. Soil Dyn Earthquake Eng 1995;14(1):59–71.
[11] Stamatopoulos C, Velgaki E, Sarma S. Sliding-block back analysis of earthquake-induced slides. Soils Found 2000;40(6):61–75.
[12] Stamatopoulos CA. Sliding system predicting large permanent co-seismic movements of slopes. Earthquake Eng Struct Dyn 1996;25(10):1075–93.
[13] Sarma S.K., Chlimintzas G.O. Co-seismic and post seismic displacement of slopes. In: Proceedings of the XV ICSMEG TC4, satellite conference on “lesson learned from recent strong earthquakes”, Istanbul; 2001. p. 183–188.
[14] Stamatopoulos CA, Mavromihalis C, Sarma S. Correction for geometry changes during motion of sliding-block seismic displacement. J Geotech Geoenviron Eng ASCE 2011;137(10):926–38.
[15] Stamatopoulos CA, Velgaki EG, Modaressi A, Lopez-Caballero F. Seismic displacement of gravity walls by a two body model. Bull Earthquake Eng 2006;4:295–318.
[16] Biondi G, Cascone E, Maugeri M. Displacement versus pseudo-static evaluation of the seismic performance of sliding retaining walls. Bull Earthquake Eng 2014;12(3):1239–67 (2014).
[17] Stamatopoulos CA. Constitutive modelling of earthquake-induced slides on clays along slip surface. Landslides 2009;6(3):191–207.
[18] Stamatopoulos CA. Prediction of the seismic displacement of landslides using a multi-block model. Landslides Causes Types Effects 2010:225–50.
[19] Stamatopoulos CA, Di B. Simplified multi-block constitutive model predicting earthquake-induced landslide triggering and displacement along slip surfaces of saturated sand. Soil Dyn Earthquake Eng 2014;67(1):16–29.
[20] Bandini V., Cascone E., Biondi G.A. GLE multi-block model for the evaluation of seismic displacements of slopes. In: Proceedings of the seismic engineering international conference commemorating the 1908 Messina and Reggio Calabria Earthquake, Reggio Calabria; 2008. vol. 1, p. 485–492.
[21] Bandini V., Cascone E., Biondi G. Multi-block seismic displacement analysis of the 1980 Calitri landslide. In: Proceedings of the second international conference on performed-based design in earthquake geotechnical engineering, Taormina, Italy; 2012.
[22] Bandini V., Biondi G., Cascone E. Seismic displacement analysis of slopes: comparison between a multi-block model and shaking table tests. In: Proceedings of the fifth international conference on earthquake geotechnical engineering, Santiago, Chile; 2011.
[23] Crespellani T, Ghinelli A, Madiai C, Vannucchi G. Analisi di stabilità dei pendii naturali in condizioni sismiche. Rivista Italiana di Geotecnica 1990;XXIV (2):49–74.
[24] Crespellani T, Madiai C, Maugeri M. Analisi di stabilità di un pendio in condizioni sismiche e post-sismiche. Rivista Italiana di Geotecnica 1996; XXX(1):50–61.
[25] Biondi G., Cascone E., Maugeri M. Seismic response of submerged cohesionless slopes. In: Proceedings of the fourth international conference on recent advances in geotechnical earthquake engineering and soil dynamics, San Diego, USA; 2001.
[26] Deng J, Tsutsumi Y, Kameya H, Koseki J. A modified procedure to evaluate earthquake-induced displacements of slope containing a weak layer. Soils Found 2010;50(3):413–20.
[27] Bandini V. Analisi dei fenomeni di instabilità sismica dei pendii attraverso un modello multiblocco (Seismic stability analysis of slopes with multi-block model). PhD thesis, Dept. Civil Engineering, University of Messina, Italy, (in Italian); 2008.
[28] Sarma SK. Response and stability of earth dams during strong earthquakes. (Miscellaneous paper GL-79-13). Vicksburg: U.S. Army engineer Waterways Experiment Station,; 1979.
[29] Fredlund DG, Krahn J. Comparison of slope stability methods of analysis. Can Geotech J 1977;14:429–39.
[30] Wartman J, Seed RB, Bray JD. Shaking table modeling of seismically induced deformations in slopes. J Geotech Geoenviron Eng ASCE 2005;131(5):610–22.
[31] Simonelli A.L., Di Stefano P. Effects of vertical seismic accelerations on slope displacements. In: Proceedings of the IV international conference on recent advances in geotechnical earthquake engineering and soil dynamics, San Diego, CA; 2001.
[32] Krahn J. Stability modelling with slope/W—an engineering methodology; 2004.
[33] Matsui T, Ohara H, Ito T. Cyclic stress–strain history and shear characteristics of clay. J Geotech Eng ASCE 1980;106(10):1101–20.
[34] Matasovic N, Vucetic M. Generalized cyclic-degradation-pore pressure generation model for clays. J Geotech Eng Div ASCE 1995;121(1):33–42.
[35] Vucetic M. Cyclic threshold shear strain in soils. J Geotech Eng ASCE 1994;120 (12):2208–28.
[36] Idriss IM, Dobry R, Singh AM. Nonlinear behaviour of soft clays during cyclic loading. J Geotech Eng ASCE 1978;104(12):1427–47.
[37] Ishihara K. Soil behaviour in earthquake geotechnics. Oxford engineering science series. USA: Oxford University Press; 1996.
[38] Seed H.B., Idriss I.M., Makdisi F., Banerjee N. Representation of irregular stress time histories by equivalent uniform stress series in liquefaction analysis. Report EERC, 75-29. Earthquake Engineering Research Center, University of California; 1975.
[39] Liu AH, Stewart JP, Abrahamson NA, Moriwaki Y. Equivalent number of uniform stress cycle for soil liquefaction analysis. J Geotech Eng ASCE 2001;127(12):1017–26.
[40] Biondi G., Cascone E., Maugeri M. Number of uniform stress cycles equivalent to seismic loading. In: Proceedings of the 11th international conference on soil dynamics & earthquake engineering and third international conference on earthquake geotechnical engineering, Berkeley; 2004 (CD-Rom).
[41] Biondi G, Cascone E, Di Filippo G. Affidabilità di alcune correlazioni empiriche per la stima del numero di cicli di carico equivalente. Rivista Italiana di Geotecnica 2012;XLVI(2):9–39.
[42] Kim J, Riemer M, Bray JD. Dynamic properties of geosynthetic interfaces. Geotech Test J 2005;28(3):1–9.
[43] Idriss IM, Boulanger RW. Soil liquefaction during earthquakes. Earthquake Engineering Research Institute; 2008.

[44] Trifunac MD, Brady AG. A study of the duration of strong earthquake ground motion. Bull Seismol Soc Am 1975;65:581–626.
[45] Rathje EM, Abrahamson NA, Bray JD. Simplified frequency content estimates of erthquake ground motions. J Geotech Geoenviron Eng ASCE 1998;124 (2):150–9.
[46] Araya R., Saragoni R. Earthquake accelerogram destructiveness potential factor. In: Proceedings of the eightth WCEE, San Francisco, 1984; 2: 835-841.
[47] Wartman J., Seed R.B., Bray J.D. Physical model studies of seismically induced deformations in slopes. Geo engineering report no. UCB/GT/01-01, Geo-Engineering Department of Civil and Environmental Engineering University of California, Berkeley; 2001.
[48] Kim D. Multi-scale assessment of geotextile-geomembrane interaction. PhD thesis, Dept. of Civil and Environmental Engineering, Georgia Institute of Technology; 2006.